Polarization-filtering and polarization-maintaining low-loss negative curvature fibers

CHENGLI WEI,[1] CURTIS R. MENYUK,[2] AND JONATHAN HU[1,*]

[1]*Baylor University, One Bear Place #97356, Waco, Texas 76798, USA*
[2]*University of Maryland Baltimore County, 5200 Westland Blvd., Baltimore, MD 21227, USA*
[*]*jonathan_hu@baylor.edu*

Abstract: We propose a polarization-filtering and polarization-maintaining negative curvature fiber in which two nested resonant tubes are added to a standard negative curvature fiber with one ring of tubes. The coupling between the glass modes in the nested resonant tubes and the fundamental core modes is used to increase the birefringence and differential loss for the fundamental core modes in the two polarizations. We show computationally that the birefringence and the loss ratio between the modes in the two polarizations can reach 10^{-5} and 850, respectively. Meanwhile, the low-loss mode has a loss that is lower than 0.02 dB/m. The relatively simple design of this polarization-maintaining negative curvature fiber will be useful in hollow-core fiber devices that are sensitive to polarization effects, such as fiber lasers, fiber interferometers, and fiber sensors.

References and links

1. F. Poletti, N. V. Wheeler, M. N. Petrovich, N. K. Baddela, E. Numkam Fokoua, J. R. Hayes, D. R. Gray, Z. Li, R. Slavik, and D. J. Richardson, "Towards high-capacity fibre-optic communications at the speed of light in vacuum," Nat. Photonics **7**(4), 279–284 (2013).
2. P. K. A. Wai and C. R. Menyuk, "Polarization mode dispersion, decorrelation and diffusion in optical fibers with randomly varying birefringence," J. Lightwave Technol. **14**(2), 148–157 (1996).
3. Y. Takushima, S. Yamashita, K. Kikuchi, and K. Hotate, "Polarization-stable and single-frequency fiber lasers," J. Lightwave Technol. **16**(4), 661–669 (1998).
4. W. Burns, C. Lin, and R. Moeller, "Fiber-optic gyroscopes with broad-band sources," J. Lightwave Technol. **1**(1), 98–105 (1983).
5. J. Noda, K. Okamoto, and Y. Sasaki, "Polarization-maintaining fibers and their applications," J. Lightwave Technol. **4**(8), 1071–1089 (1986).
6. C. R. Menyuk, "Nonlinear pulse propagation in birefringent optical fibers," IEEE J. Quantum Electron. **23**(2), 174–176 (1987).
7. K. Suzuki, H. Kubota, S. Kawanishi, M. Tanaka, and M. Fujita, "Optical properties of a low-loss polarization-maintaining photonic crystal fiber," Opt. Express **9**(13), 676–680 (2001).
8. M. E. Fermann, M. J. Andrejco, Y. Silberberg, and M. L. Stock, "Passive mode locking by using nonlinear polarization evolution in a polarization-maintaining erbium-doped fiber," Opt. Lett. **18**(11), 894–896 (1993).
9. A. D. Kim, J. N. Kutz, and D. J. Muraki, "Pulse-train uniformity in optical fiber lasers passively mode-locked by nonlinear polarization rotation," IEEE J. Ouantum Electron. **36**(4), 465–471 (2000).
10. M. Salhi, H. Leblond, and F. Sanchez, "Theoretical study of the erbium-doped fiber laser passively mode-locked by nonlinear polarization rotation," Phys. Rev. A **67**(1), 013802 (2003).
11. R. F. Cregan, B. J. Mangan, J. C. Knight, T. A. Birks, P. St. J. Russell, P. J. Roberts, and D. C. Allan, "Single mode photonic band gap guidance of light in air," Science **285**(5433), 1537–1539 (1999).
12. J. Broeng, S. E. Barkou, T. Sndergaard, and A. Bjarklev, "Analysis of air-guiding photonic bandgap fibers," Opt. Lett. **25**(2), 96–98 (2000).
13. C. Wei, R. J. Weiblen, C. R. Menyuk, and J. Hu, "Negative curvature fibers," Adv. Opt. Photon. **9**(3), 504–561 (2017).
14. J. C. Knight, J. Broeng, T. A. Birks, and P. St. J. Russell, "Photonic band gap guidance in optical fibers," Science **282**(5393), 1476–1478 (1998).
15. K. Saitoh and M. Koshiba, "Photonic bandgap fibers with high birefringence," IEEE Photon. Technol. Lett. **282**(9), 1291–1293 (2002).

16. G. Bouwmans, F. Luan, J. C. Knight, P. St. J. Russell, L. Farr, B. J. Mangan, and H. Sabert, "Properties of a hollow-core photonic bandgap fiber at 850 nm wavelength," Opt. Express **11**(14), 1613–1620 (2003).
17. X. Chen, M. J. Li, N. Venkataraman, M. T. Gallagher, W. A. Wood, A. M. Crowley, J. Carberry, L. A. Zenteno, and K. W. Koch, "Highly birefringent hollow-core photonic bandgap fiber," Opt. Express **12**(16), 3888–3893 (2004).
18. J. M. Fini, J. W. Nicholson, B. Mangan, L. Meng, R. S. Windeler, E. M. Monberg, A. DeSantolo, F. V. DiMarcello, and K. Mukasa, "Polarization maintaining single-mode low-loss hollow-core fibres," Nat. Commun. **5**, 5085 (2014).
19. Y. Wang, F. Couny, P. J. Roberts, and F. Benabid, "Low loss broadband transmission in optimized core-shape Kagome hollow-core PCF," in *Conference on Lasers and Electro-Optics 2010*, OSA Technical Digest (CD) (Optical Society of America, 2010), paper CPDB4.
20. Y. Y. Wang, N. V. Wheeler, F. Couny, P. J. Roberts, and F. Benabid, "Low loss broadband transmission in hypocycloid-core Kagome hollow-core photonic crystal fiber," Opt. Lett. **36**(5), 669–671 (2011).
21. A. D. Pryamikov, A. S. Biriukov, A. F. Kosolapov, V. G. Plotnichenko, S. L. Semjonov, and E. M. Dianov, "Demonstration of a waveguide regime for a silica hollow-core microstructured optical fiber with a negative curvature of the core boundary in the spectral region > 3.5 μm," Opt. Express **19**(2), 1441–1448 (2011).
22. F. Yu, W. J. Wadsworth, and J. C. Knight, "Low loss silica hollow core fibers for 3–4 μm spectral region," Opt. Express **20**(10), 11153–11158 (2012).
23. W. Belardi and J. C. Knight, "Hollow antiresonant fibers with low bending loss," Opt. Express **22**(8), 10091–10096 (2014).
24. F. Poletti, "Nested antiresonant nodeless hollow core fiber," Opt. Express **22**(20), 23807–23828 (2014).
25. C. Wei, R. A. Kuis, F. Chenard, C. R. Menyuk, and J. Hu, "Higher-order mode suppression in chalcogenide negative curvature fibers," Opt. Express **23**(12), 15824–15832 (2015).
26. P. Uebel, M. C. Günendi, M. H. Frosz, G. Ahmed, N. N. Edavalath, J.-M. Ménard, and P. St. J. Russell, "Broadband robustly single-mode hollow-core PCF by resonant filtering of higher-order modes," Opt. Lett. **41**(9), 1961–1964 (2016).
27. L. Vincetti and V. Setti, "Elliptical hollow core tube lattice fibers for terahertz applications," Opt. Fiber Technol. **19**(1), 31–34 (2013).
28. W. Ding and Y. Y. Wang, "Hybrid transmission bands and large birefringence in hollow-core anti-resonant fibers," Opt. Express **23**(16), 21165–21174 (2015).
29. S. A. Mousavi, S. R. Sandoghchi, D. J. Richardson, and F. Poletti, "Broadband high birefringence and polarizing hollow core antiresonant fibers," Opt. Express **24**(20), 22943–22958 (2016).
30. C. Wei, C. Menyuk, and J. Hu, "Bending-induced mode non-degeneracy and coupling in chalcogenide negative curvature fibers," Opt. Express **24**(11), 12228–12239 (2016).
31. A. F. Kosolapov, G. K. Alagashev, A. N. Kolyadin, A. D. Pryamikov, A. S. Biryukov, I. A. Bufetov, and E. M. Dianov, "Hollow-core revolver fibre with a double-capillary reflective cladding," Quantum Electron. **46**(3), 267–270 (2016).
32. W. Belardi, "Design and properties of hollow antiresonant fibers for the visible and near infrared spectral range," J. Lightwave Technol. **33**(21), 4497–4503 (2015).
33. J. E. Antonio-Lopez, S. Habib, A. V. Newkirk, G. Lopez-Galmiche, Z. S. Eznaveh, J. C. Alvarado-Zacarias, O. Bang, M. Bache, A. Schülzgen, and R. A. Correa, "Antiresonant hollow core fiber with seven nested capillaries," in *2016 IEEE Photonics Conference (IPC)*, Waikoloa, HI, 2016, pp. 402–403.
34. C. Wei, C. R. Menyuk, and J. Hu, "Impact of cladding tubes in chalcogenide negative curvature fibers," IEEE Photon. J. **8**(3), 2200509 (2016).
35. C. Wei, J. Hu, and C. R. Menyuk, "Comparison of loss in silica and chalcogenide negative curvature fibers as the wavelength varies," Front. Phys. **4**, 30 (2016).
36. M. Michieletto, J. K. Lyngs, C. Jakobsen, J. Lgsgaard, O. Bang, and T. T. Alkeskjold, "Hollow-core fibers for high power pulse delivery," Opt. Express **24**(7), 7103–7119 (2016).
37. K. Saitoh and M. Koshiba, "Leakage loss and group velocity dispersion in air-core photonic bandgap fibers," Opt. Express **11**(23), 3100–3109 (2003).
38. N. M. Litchinitser, A. K. Abeeluck, C. Headley, and B. J. Eggleton, "Antiresonant reflecting photonic crystal optical waveguides," Opt. Lett. **27**(18), 1592–1594 (2002).
39. A. V. Newkirk, J. E. Antonio-Lopez, J. Anderson, R. Alvarez-Aguirre, Z. S. Eznaveh, G. Lopez-Galmiche, R. Amezcua-Correa, and A. Schülzgen, "Modal analysis of antiresonant hollow core fibers using S^2 imaging," Opt. Lett. **41**(14), 3277–3280 (2016).
40. J. R. Hayes, S. R. Sandoghchi, T. D. Bradley, Z. Liu, R. Slavik, M. A. Gouveia, N. V. Wheeler, G. Jasion, Y. Chen, E. N. Fokoua, M. N. Petrovich, D. J. Richardson, and F. Poletti, "Antiresonant hollow core fiber with an octave spanning bandwidth for short haul data communications," J. Lightwave Technol. **35**(3), 437–442 (2017).
41. D. J. Richardson, J. Nilsson, and W. A. Clarkson, "High power fiber lasers: current status and future perspectives [Invited]," J. Opt. Soc. B **27**(11), B63–B92 (2010).
42. C. Xu and F. W. Wise, "Recent advances in fibre lasers for nonlinear microscopy," Nat. Photonics **7**(11), 875–882 (2013).
43. X. Zheng, B. Debord, L. Vincetti, B. Beaudou, F. Gérôme, and F. Benabid, "Fusion splice between tapered inhibited coupling hypocycloid-core Kagome fiber and SMF," Opt. Express **24**(13), 14642–14647 (2016).

1. Introduction

Polarization effects play an important role in many applications, such as optical communication networks, fiber lasers, fiber gyroscopes, and interferometric devices [1–5]. In optical fibers, fabrication imperfections and environmental perturbations, such as bending and twisting will introduce a random birefringence and lead to an unpredictable output [3, 6]. In fiber devices, unwanted birefringence will lead to different behavior in the two polarization eigenmodes [3], and mode competition between the two modes can lead to polarization instability [3]. To mitigate this effect, one can use polarization-maintaining fibers, in which the unpredictable polarization evolution is eliminated. These fibers have high birefringence, so that light propagates in only one polarization [5, 7]. Polarization effects are also used to make fast saturable absorbers in passively mode-locked fiber lasers [8–10]. When an intense optical pulse propagates in an optical fiber, the polarization state in the high-intensity peak will be different from the low-intensity wings, allowing the low-intensity wings to be attenuated by a polarization filter. Here, we show computationally that fiber devices that both filter and maintain the polarization can be implemented in negative curvature fibers, thereby enabling efficient and compact all-fiber devices.

Hollow-core photonic crystal fibers can transmit light with low loss of about 1 dB/km while delivering high-power millijoule pulses with low nonlinearity [11–13]. A photonic bandgap structure uses a periodic array of air holes in the cladding to confine light in the core [14]. In hollow-core bandgap fibers, birefringence can be induced by utilizing an asymmetric core shape [15–18]. A new kind of hollow-core fiber called negative curvature fiber has drawn much attention recently due to its attractive properties, including a low transmission loss, a wide transmission bandwidth, and a simple structure [19–26]. Several polarization-maintaining negative curvature fiber structures have already been proposed. A straightforward approach by Vincetti and Setti [27] is to use a negative curvature fiber whose cladding is composed of an elliptical arrangement of cladding tubes. The birefringence in this case is always low when the wavelength is close to the center of the transmission windows [27]. Ding *et al.* [28] showed that high birefringence can be achieved in negative curvature fibers by using tubes with slightly different thicknesses in two transverse orthogonal directions. Mousavi *et al.* [29] proposed a structure that uses resonant and antiresonant tubes in two orthogonal directions to induce high birefringence. In this design, doubly-nested antiresonant tubes are required to confine the mode and achieve a low leakage loss.

In this paper, we aim to design a relatively simple negative curvature fiber with a high birefringence and a high differential loss between the fundamental core modes in the two polarizations. We show two structures in the Fig. 1 to illustrate the main idea. Figure 1(a) shows a negative curvature fiber with two larger tubes in the y-direction, which are used to increase the birefringence and differential loss by coupling the fundamental core mode in one polarization to the tube mode, as indicated by the red-highlighted profile. Our simulation results show that the fundamental core modes in the x- and y-polarizations have similar effective indices even with an asymmetric core profile, which is consistent with other published results [27, 29, 30]. The tube modes in the x- and y-polarizations also have very similar effective indices. Coupling between the tube modes and the core modes in the two polarizations occurs within the same parameter range. Hence, this design leads to fibers with a small birefringence and a small differential loss between the fundamental core modes in the two polarizations.

Our goal is to find a fiber structure where the coupling between the cladding modes and the fundamental core modes in the two polarizations occurs within different parameter ranges. Figure 1(b) shows a negative curvature fiber structure with two nested tubes in the y-direction using a wall thickness close to the resonance condition. Negative curvature fibers with one nested tube in each major tube have been fabricated [31–33]. With proper design, the effective indices and mode profiles of the glass modes will be different for the x- and y-polarizations. The novelty in our design is the use of the coupling between the glass modes in the nested resonant tubes and
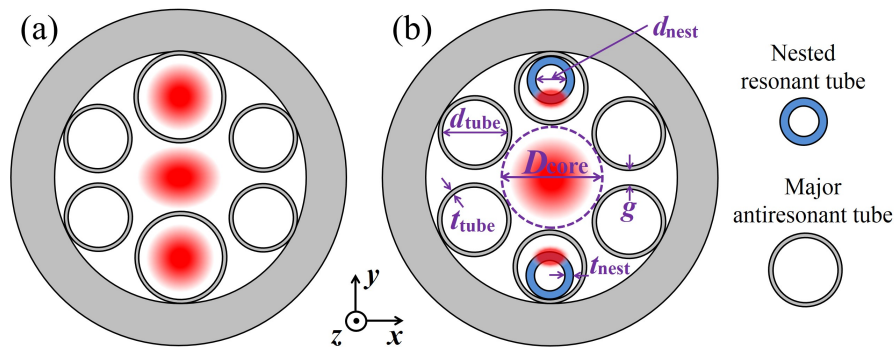
Fig. 1. Schematic illustration of two negative curvature fibers with asymmetric geometries. Red-highlighted regions indicate locations where the mode intensity is high. (a) Coupling between the fundamental core mode and tube mode. (b) Coupling between the fundamental core mode and glass mode.

the fundamental core mode to increase the birefringence and the differential loss between modes in two polarizations. The physics and mechanism for the proposed fiber design are different from those in previous works on polarization-maintaining negative curvature fibers [28, 29]. As long as all the major tubes are antiresonant, the loss for the other polarization is still low and comparable to the loss of standard negative curvature fibers with one ring of antiresonant tubes.

2. Geometry

Three mode types exist in negative curvature fibers: core modes, tube modes, and glass modes. Core modes reside primarily in central air-core of the fiber, while tube modes reside primarily in the air inside the cladding tubes. These modes are antiresonantly guided when the tube glass thickness, t, satisfies the antiresonance condition $t = (m - 0.5)\lambda/[2(n_1^2 - n_0^2)^{1/2}]$, where m equals any positive integer [24, 25]. The glass modes are guided by glass, although they extend into the air. Because the guidance mechanism for glass and tube modes is different, the variation of their effective indices as the glass thickness changes is different. A slight change in the glass thickness leads to a large change in the effective index of the glass modes, while only slightly affecting the tube modes.

The geometry of the proposed polarization-maintaining negative curvature fiber is shown in Fig. 1(b). The two nested resonant tubes in the y-direction are represented by blue rings. The tube diameter, d_{tube}, the core diameter, D_{core}, the wall thickness of the major tube, t, and the minimum gap distance between the cladding tubes, g, are related by the expression: $D_{\text{core}} = d_{\text{tube}} + 2t + 2g$ for fibers with 6 major tubes [30, 34–36]. We calculate the fiber modes and propagation constants using Comsol Multiphysics, a commercial full-vector mode solver based on the finite-element method. Anisotropic, perfectly matched layers (PMLs) are positioned outside the cladding in order to reduce the size of the simulation window [37]. We simulate silica glass with a refractive index of 1.444 at a wavelength of 1550 nm for polarization-maintaining fibers [7, 18, 29]. The core diameter, D_{core}, is 50 μm, which is around 30 times larger than the transmission wavelength [21, 22, 36]. A major tube diameter of 30 μm is used throughout this paper, unless otherwise indicated. The wall thickness of the major tubes, t, is 1.12 μm to satisfy the antiresonance condition, $t = (m - 0.5)\lambda/[2(n_1^2 - n_0^2)^{1/2}]$ where n_1 and n_0 are the refractive indices of the glass and air, λ is the light wavelength, and m is the order of antiresonance [13, 38]. We use the second antiresonance transmission band for which $m = 2$ with a glass thickness of 1.12 μm, corresponding to typical glass thicknesses that have been drawn in the past [32, 39]. A

higher-order antiresonance implies a thicker tube wall, especially for shorter wavelengths, which makes fabrication easier. Geometries that use tube thicknesses corresponding to the first, second, or third antiresonance have similar minimum losses in the transmission band [34, 35].

3. Loss in the two polarization modes

In standard negative curvature fibers with one ring of antiresonant tubes, the loss due to the surface scattering is two orders of magnitude lower than the confinement loss [24, 40] and is not taken into account in this work. We study the mode loss in the two polarizations for the geometry that is shown in Fig. 1(b). Coupling can be induced between the glass modes and the fundamental core modes in each of the two polarizations by tuning the wall thickness of the nested tubes. This new mechanism to induce high birefringence has not been used in previous designs of polarization-maintaining fibers. Figure 2(a) shows the effective index of the fundamental core modes in both the x- and y-polarizations as a function of the thickness of the nested tube, t_{nest}. The ratio of the nested tube diameter to the major tube diameter, d_{nest}/d_{tube}, is 0.7. There are several avoided crossings when the thickness of the nested tube increases from 1.50 μm to 1.53 μm near the resonance thickness, $t = m\lambda/[2(n_1^2 - n_0^2)^{1/2}]$, where the resonance order $m = 2$ is used. The corresponding losses are shown in Fig. 2(c). There are several high-loss peaks in the x- and y-polarizations, corresponding to the avoided crossings in Fig. 2(a). The avoided crossings or high-loss peaks of the modes in the x- and y-polarizations occur at different nested tube thicknesses, t_{nest}. The difference between the nested tube thicknesses of the x- and y-polarizations at the first high-loss peaks is denoted by Δt_{nest} in Fig. 2(c). We show similar plots of the effective index and loss in Figs. 2(b) and 2(d), where the ratio of the nested tube diameter
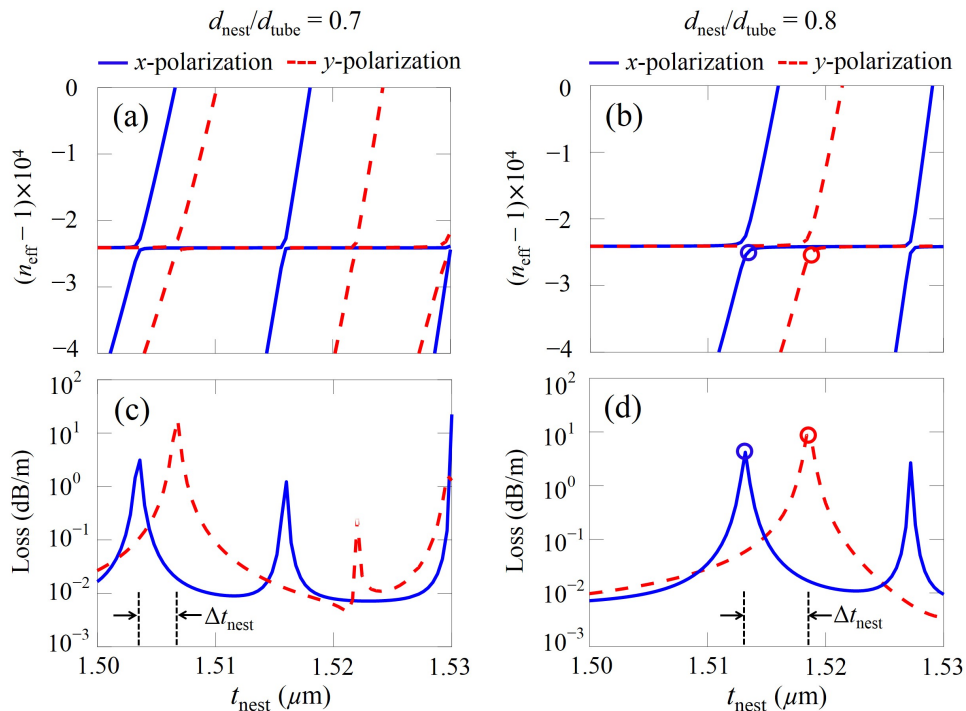

Fig. 2. (a), (b) Effective index and (c), (d) loss of modes in the x- and y-polarizations as a function of t_{nest}. (a), (c) $d_{nest}/d_{tube} = 0.7$. (b), (d) $d_{nest}/d_{tube} = 0.8$.
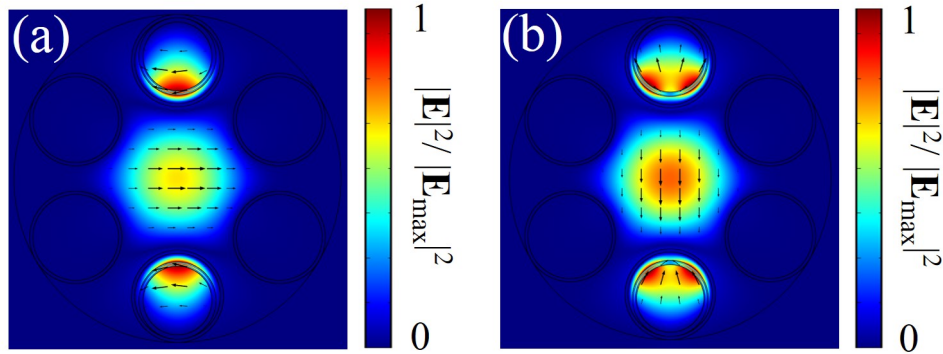
Fig. 3. (a) Normalized mode intensity in the x-polarization at t_{nest} = 1.513 μm and (b) normalized mode intensity in the y-polarization at t_{nest} = 1.519 μm with d_{nest}/d_{tube} = 0.8, corresponding to the blue and red circles in Figs. 2(b) and 2(d).

to the major tube diameter, d_{nest}/d_{tube}, is 0.8. The difference between the nested tube thicknesses, Δt_{nest}, in the fiber using d_{nest}/d_{tube} = 0.8 is larger than that in the fiber using d_{nest}/d_{tube} = 0.7.

The mode fields in the coupling region are shown in Fig. 3, corresponding to the high-loss peaks in the x- and y-polarizations, denoted by blue and red circles in Fig. 2(d). The wavelength is 1550 nm. The color indicates the electric field intensity, normalized to its maximum. The arrows indicate the direction of the transverse electric field and the lengths of the arrows are proportional to the amplitude of the transverse electric field. For the mode in the x-polarization shown in Fig. 3(a), the core mode couples with the glass mode, which has a maximum at one point in both nested tubes. For the mode in the y-polarization shown in Fig. 3(b), the core mode couples with the glass mode, which has a maximum at two points in both nested tubes.

4. Structure optimization

Figures 2 and 3 show coupling between the glass modes and the fundamental core modes. When the coupling is strong, there is a high differential loss between the fundamental core modes in the x- and y-polarizations. Due to uncertainty in the fiber drawing process, it is desirable to design a fiber with the largest possible separation, Δt_{nest}, in order to increase the fabrication tolerance. Here, we study the impact on the parameter Δt_{nest} from the major tube diameter, d_{tube}, and the ratio of the nested tube diameter to the major tube diameter, d_{nest}/d_{tube}. We show a contour plot of the parameter Δt_{nest} in Fig. 4. The wavelength is 1550 nm. Each value of Δt_{nest} on the contour plot is obtained from the leakage loss curves of the modes in the x- and y-polarizations as a function of nested tube thickness, t_{nest}, that is shown in Fig. 2. Figure 4 shows that the parameter Δt_{nest} increases when the tube diameter, d_{tube}, decreases or the ratio of the nested tube diameter to major tube diameter, d_{nest}/d_{tube}, increases. Hence, a fiber with a smaller major tube diameter and a larger nested tube diameter yields a larger Δt_{nest}. A stronger interaction between nested and major tubes leads to a larger separation Δt_{nest} because the mode intensity in the nested tubes reaches its maximum at different locations for the two polarizations, as shown in Figs. 3(a) and 3(b). We use a maximum d_{nest}/d_{tube} of 0.8 since it may be difficult to fabricate a fiber with d_{nest}/d_{tube} > 0.8. A small gap between the nested and major tubes may collapse in the fiber drawing process.

Figure 5 shows the loss of the fundamental core modes in the x- and y-polarizations as a function of d_{nest}/d_{tube} when the glass mode and the fundamental core mode are resonantly coupled in the y-polarization. The corresponding thickness of the nested tube, t_{nest}, is also plotted using a green dotted curve. The diameter of the major tube, d_{tube}, is fixed at 30 μm. Setting d_{nest}/d_{tube}
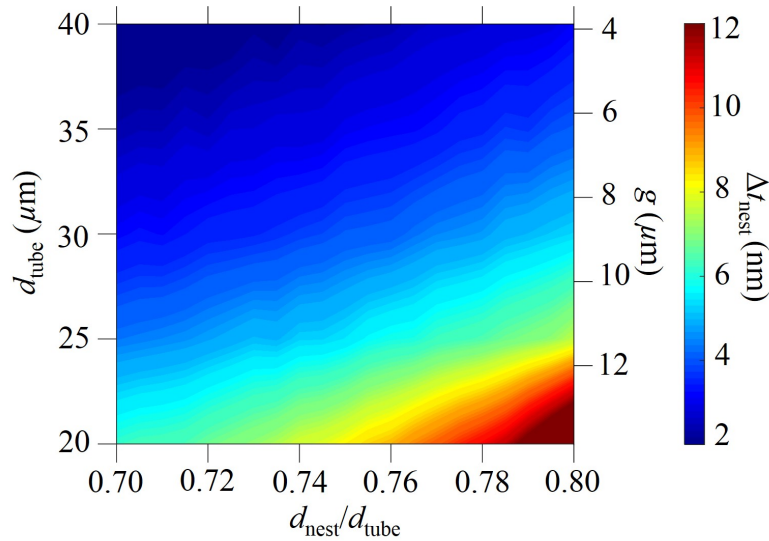
Fig. 4. Contour plot of Δt_{nest} as a function of d_{tube} and d_{nest}/d_{tube}. The corresponding gap, g, is also marked on the right side of the contour plot.
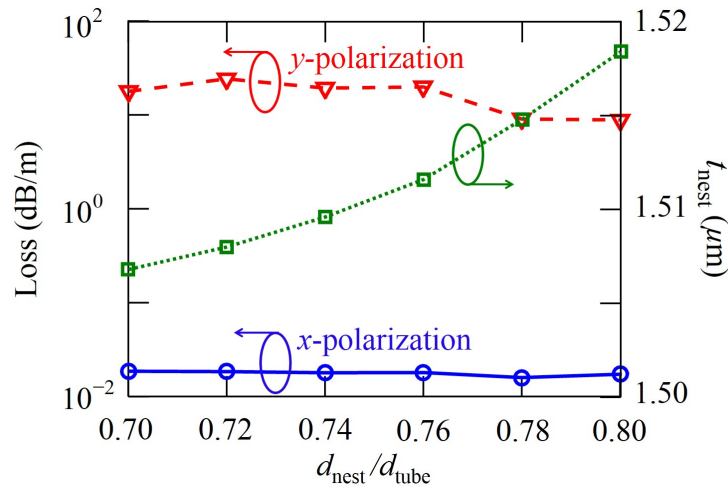

Fig. 5. Loss of modes in the x- and y-polarizations and the thickness of the nested tube, t_{nest}, when the glass mode and the core mode in the y-polarization are resonantly coupled. The diameter of the major tube, d_{tube}, is 30 μm.

= 0.8 in order to maximize Δt_{nest}, we find that t_{nest} = 1.519 μm. This value corresponds to the red circles in Figs. 2(b) and 2(d). When d_{nest}/d_{tube} is between 0.7 and 0.8, the loss of the x-polarization is below 0.02 dB/m. The loss ratio of the y-polarization to the x-polarization is more than 500 within the parameter range that we show in Fig. 5.

We also carried out additional simulations to compare the results of fibers using six, eight, and ten cladding tubes. For all these fibers, we set the core diameter, tube wall thickness, and wavelength equal to 50 μm, 1.12 μm, and 1.55 μm, respectively. The tube diameters are 30 μm, 25 μm, and 15 μm in the fibers with six, eight, and ten cladding tubes, respectively. Different
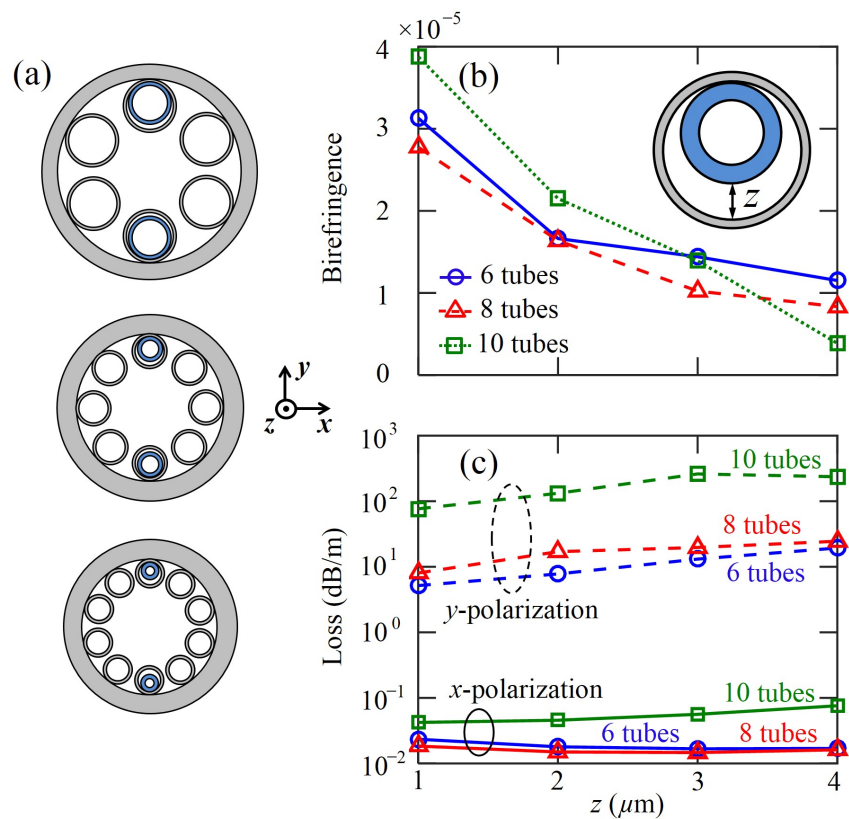
Fig. 6. (a) Schematics illustration, (b) birefringence, and (c) loss of negative curvature fibers with six, eight, and ten cladding tubes. Inset in (b) shows a schematic illustration of the maximum distance, z, between the major antiresonant tube and the nested resonant tube.

thicknesses of the nested tube are selected to give the maximum birefringence. Figure 6(b) shows the birefringence as a function of the maximum distance, z, between the major antiresonant tube and the nested resonant tube. The birefringence in these three fibers are on the same scale. The birefringence increases when z decreases; when z is smaller, a stronger interaction between nested and major tubes leads to a larger birefringence. Figure 6(c) shows the loss in both the x- and y-polarizations. The loss of the x-polarization is between 10^{-2} dB/m and 10^{-1} dB/m, which is more than two orders of magnitude lower than the loss of the y-polarization.

We also ran additional simulations for different structures to compare their performance to the performance of our fiber design, shown in Fig. 1(b). Fibers with different tube wall thickness corresponding to the first and the second antiresonance bands have a similar loss ratio and birefringence. Fibers in which antiresonant tubes are added in the four major tubes in the x-direction show a lower minimum loss in x-polarization and a similar birefringence. Fibers that are modified by removing the nested resonant tubes in the y-direction and adding four nested resonant tubes in the x-direction have a low loss ratio between the two polarization modes. We include figures and corresponding descriptions in the appendix that describe additional designs and fabrication tolerance.
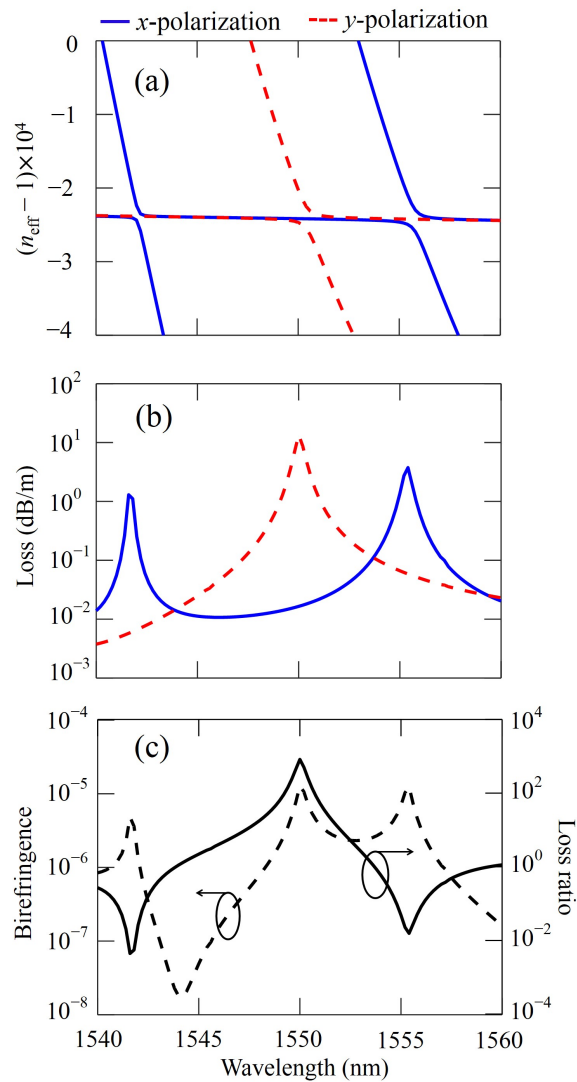
Fig. 7. (a) Effective index, (b) loss, (c) birefringence, and loss ratio as a function of wavelength.

5. Performance comparison of polarization-maintaining negative curvature fibers

In this section, we study the performance of the fiber as a function of wavelength. The ratio of the nested tube diameter to the major tube diameter, d_{nest}/d_{tube}, is 0.8, and the thickness of the nested tube, t_{nest}, is 1.519 μm, based on Fig. 2. Figures 7(a) and 7(b) show the effective index and the leakage loss of the modes in the x- and y-polarizations as a function of wavelength. There is a high-loss peak in the y-polarization at the wavelength of 1550 nm between the two high-loss peaks in the x-polarization. The loss of the mode in the x-polarization is less than 0.02 dB/m when the wavelength is 1550 nm. Figure 7(c) shows the birefringence and loss ratio of the mode in the y-polarization to the mode in the x-polarization, which can reach 10^{-5} and 850, respectively, at a wavelength of 1550 nm. This fiber has a bandwidth of 1.5 nm for a loss

Table 1. Performance comparison between simulation results from different fiber designs

	Ref. [27]	Ref. [28]	Ref [29]	This paper
Loss	0.04 dB/m	0.34 dB/m	0.04 dB/m	0.02 dB/m
Loss ratio	~2	~10	1×10^3	850
# of tubes	$8(1) + 0(1/2)$	$0(1) + 12(1/2)$	$12(1) + 0(1/2)$	$8(1) + 0(1/2)$
Max. # of layers	1	3	3	2
Core shape	Ellipse	Circle	Circle	Circle
Birefringence	$< 7 \times 10^{-5}$	1×10^{-4}	1.5×10^{-4}	1.3×10^{-5}

ratio higher than 100 and a bandwidth of 4.7 nm for a loss ratio higher than 10, which can be used for polarization-filtering in a fiber laser [41, 42]. The narrow bandwidth will automatically select the specific wavelength in a fiber laser loop.

In Table 1, we show a performance comparison between the results in this paper and other simulations of polarization-maintaining negative curvature fibers, including loss, the loss ratio between the two polarization modes, the number of cladding tubes, the maximum number of layers in the azimuthal direction, the core shape, and birefringence. In some cases, half tubes are used in the geometry [28]. We write the number of tubes in the format of $p(1) + q(1/2)$, where p represents number of full tubes and q represents number of half tubes. The maximum number of antiresonant or resonant layers in any azimuthal direction is specified since a simple structure with fewer layers is easier to fabricate. Currently, nested negative curvature fibers, which have been fabricated, only have at most two glass layers in any azimuthal direction [31–33]. The fiber core shape is also compared because a circular core shape is easier to draw due to surface tension in the fiber drawing process. The fiber design that we propose in this paper only has two glass layers in any azimuthal direction and has a circular core shape. The proposed design has a relatively low leakage loss and a high loss ratio between the two polarization modes. Although the birefringence in our proposed structure is lower than in other fiber designs in Table 1, these other designs require either three glass layers in any azimuthal direction or a non-circular core shape. The feasibility of fabricating these more complex structures has not yet been demonstrated [31–33].

A commonly used approach to obtain fast saturable gain in passively mode-locked lasers is to combine nonlinear polarization rotation with a polarization filter [8–10]. In this approach, the nonlinear polarization rotation and the polarization filtering using a polarizer are usually implemented separately [8–10]. Our fiber design makes it possible to combine the nonlinear polarization rotation and polarization filtering in one device by splicing a standard fiber with our proposed fiber design, and thus enable lower-loss and more efficient fiber laser designs. The fusion splice between tapered negative curvature fibers and step-index fibers has been reported to have a total insertion loss of less than 0.5 dB [43].

6. Conclusion

In this paper, we propose a polarization-filtering and polarization-maintaining negative curvature fiber that includes two nested resonant tubes. The coupling between the glass modes in the nested resonant tubes and the fundamental core modes is used to increase the birefringence and the differential loss between the fundamental core modes in the two polarizations, while one polarization mode still has low loss. The low-loss mode has a leakage loss that is less than of 0.02 dB/m, and the loss ratio between the fundamental core modes in the two polarizations can reach 850. The physics and mechanism for the proposed fiber design are different from those

in previous works on polarization-maintaining negative curvature fibers. The proposed design contains at most two glass layers, which has been demonstrated to be feasible to fabricate. This relatively simple design of polarization-filtering and polarization-maintaining low-loss negative curvature fibers will be useful in systems that require a polarization filter that can be integrated with other optical fibers.

Appendix A: Other designs

In this section, we study the birefringence and loss in negative curvature fibers with different designs. The figures and corresponding descriptions are provided here to support the claims in the main text.

Figure 8(a) shows schematic illustrations of fibers with and without additional nested antiresonant tubes inside the four major tubes 1, 2, 4, and 5. The red dashed curve in Fig. 8(b) shows the birefringence in the fiber with additional nested antiresonant tubes, while the blue solid curve shows the birefringence in the fiber without additional nested antiresonant tubes. The solid and dashed curves in Fig. 8(c) show the loss when the light is polarized in the x- and y-directions, respectively. The red and blue curves show the loss with and without the additional nested tubes, respectively. The minimum loss for light in the x-polarization can be decreased by a factor of 1.5 by using nested antiresonant elements. However, there is no change in the maximum birefringence.

We also investigated fiber structures in which we removed the two nested resonant tubes in the major tubes 3 and 6 and added four nested resonant tubes in the major tubes 1, 2, 4, and 5. Figures 9(a) and 9(b) show the birefringence and loss in both the x- and y-polarizations. The
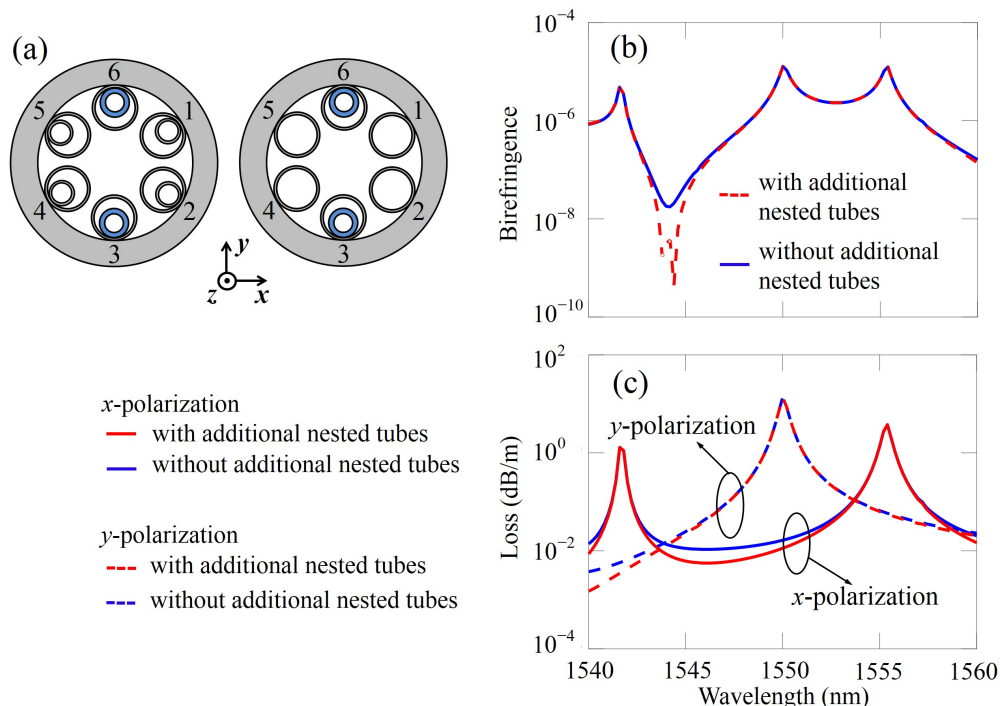

Fig. 8. (a) Schematic illustration of fibers with and without additional nested antiresonant tubes in major tubes 1, 2, 4, and 5. (b) Birefringence and (c) loss in fibers with and without additional nested antiresonant tubes.
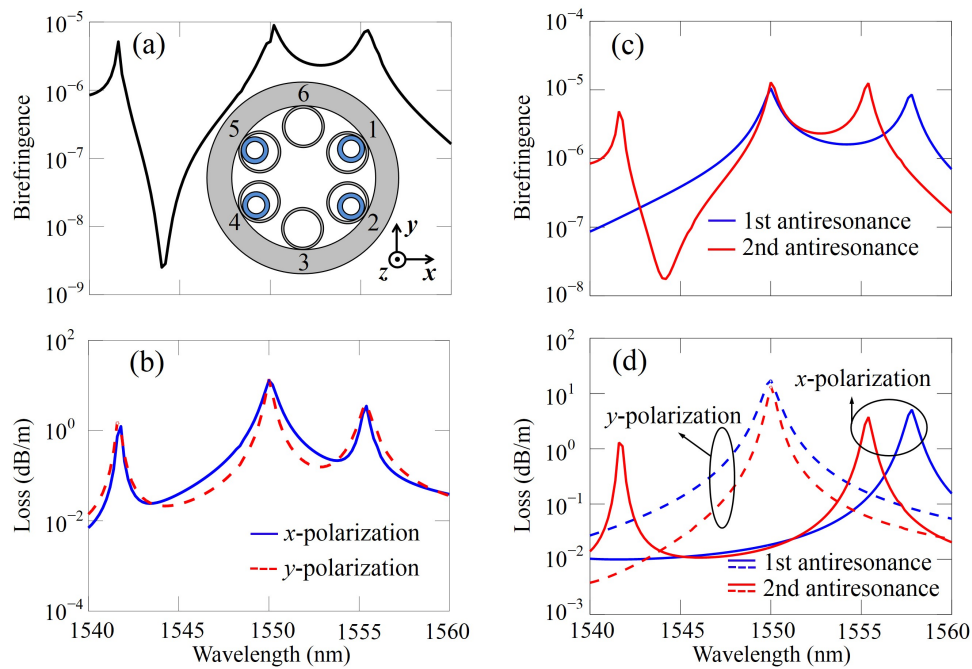
Fig. 9. (a) Birefringence and (b) loss in fibers with four nested resonant tubes, as shown in the inset. (c) Birefringence and (d) loss in the fibers with tube thicknesses corresponding to the first and the second antiresonance.

maximum birefringence is about 10^{-5}, which is the same as for the original configuration of Fig. 1. The core modes in both the x- and y-polarizations always couple to the same glass mode within the same parameter range, so that the losses in both the x- and y-polarizations are similar, and the loss ratio of the mode in the y-polarization to the mode in the x-polarization is always low.

We also compared fibers with two different tube wall thicknesses that correspond to the first and the second antiresonance. Figures 9(c) and 9(d) show that fibers using the tube wall thickness of the first or the second antiresonance have a similar birefringence and loss ratio.

Appendix B: Fabrication tolerances

In this section, we study the influence of fabrication tolerances on the performance of the fiber. We ran simulations on fibers with -10% and $+10\%$ changes of the thickness of the four major tubes 1, 2, 4, and 5. We show the birefringence and loss in Fig. 10. The variation of the tube wall thickness leads to a shift of the birefringence and transmission band. There is almost no change in either the birefringence or the loss.

We also ran simulations of fibers with an angular deviation of $5°$ of the four major tubes 1, 2, 4, and 5. The red and blue curves in Fig. 11(a) show the birefringence in the fiber with and without the $5°$ angular deviation, respectively. The solid and dashed curves in Fig. 11(b) show the loss for x- and y-polarized light, respectively. There is almost no change in either the birefringence or the loss.

The fiber proposed in the main text of this manuscript is tolerant of variations of the tube wall thickness and angular deviations of the cladding tubes. This robustness will facilitate its fabrication.
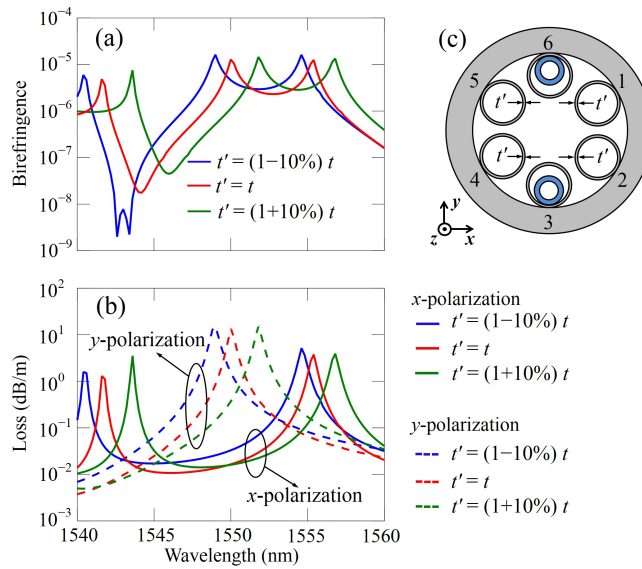
Fig. 10. (a) Birefringence and (b) loss in fibers with different tube thicknesses for the four major tubes 1, 2, 4, and 5. (c) Schematic illustration of fibers with different glass thickness, t', for the major tubes without nested tubes. The original thickness for major tubes, t, is 1.12 μm.
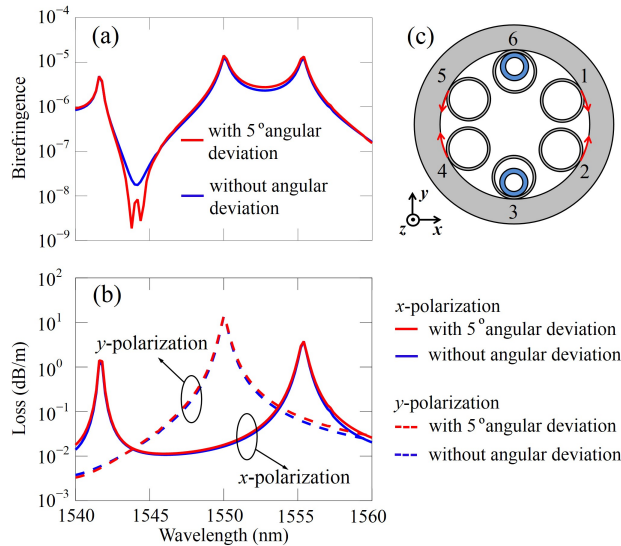

Fig. 11. (a) Birefringence and (b) loss in the fibers with and without a 5°angular deviation of the four major tubes 1, 2, 4, and 5. (c) Schematic illustration of the fiber. Arrows indicate the direction of the angular deviation.

Acknowledgments